Synchronization and Cell Search Algorithms in 3GPP Long Term Evolution Systems (FDD mode)

ABDO N. GABER [1], LOAY D. KHALAF [2], AHMAD M. MUSTAFA [2]
Electrical Engineering Department
The University of Jordan [2]
Mühlen Str. 15, 39104 Magdeburg, Germany [1]
YEMEN [1], JORDAN [2]
abdonasser@daad-alumni.de

Abstract: - In this paper initial downlink synchronization (sync) and cell identification algorithms for the 3rd generation partnership project (3GPP) long term evolution (LTE) systems are presented. The frequency division duplex (FDD) mode is used in the downlink radio frame structure. A user equipment digital receiver architecture is proposed. The orthogonality of signals in orthogonal frequency division multiplexing (OFDM) may be lost due to some impairments such as frequency, time, and phase offsets. Therefore, major parts of this research are involved in restoring the orthogonality at the user equipment (UE) by using some techniques to estimate the sync parameters, and to detect cell identity among candidate cells based on sync signals. A Farrow structure interpolator is used to compensate the fractional timing offset. Both inter site synchronous and inter site asynchronous networks are presented. Computer simulations are used to demonstrate the performance of the proposed schemes with multipath Rayleigh fading channel, frequency offsets, timing offsets, and additive white Gaussian noise (AWGN). Results show high probability of cell identification in a very short time 20 ms in both multi cell model scenarios, especially when multiple input multiple output (MIMO) technique, oversampling at the UE, and high order Farrow structure interpolator are used.

Key-Words: - 3GPP LTE, OFDM, MIMO, Frequency and Time Synchronization, Cell Search

1 Introduction

The 3GPP (3rd Generation Partnership Project) long term evolution (LTE) downlink transmission scheme was proposed based on orthogonal frequency division multiplexing (OFDM), where the major system requirements related to the physical layer are given in [1]. OFDM is an attractive choice for the downlink, especially when combined with spatial multiplexing, which is referred to as multiple input multiple output (MIMO) [2]. This is due to its inherent immunity to multipath interference (MPI) due to a low symbol rate and the use of a cyclic prefix (CP), and its support of different transmission bandwidth arrangements [3]. Multi antennas at the transmitter and receiver, MIMO technology, are used to increase the diversity gain and to enhance the system in frequency selective channels. OFDM also offers a number of potential performance advantages over a system using a single carrier frequency such as: high spectral efficiency, simple receiver design, efficiency in MIMO processing, and robustness in a multi-path environment especially in larger bandwidths. Orthogonality of OFDM might be lost at the receiver due to some impairments like frequency offsets, time offsets, phase offsets, and sampling rate changes. Therefore,

estimation of those synchronization (sync) parameters is essential for performing reliable demodulation and detection of the data from the received signal.

In order to establish communication between the user equipment (UE) and the base station (enhanced Node-B), some processes must be performed by the UE [3]. The first process is called cell search, during which the UE has to check for the strongest signal coming from the nearest base station to perform sync, and achieve cell identity (ID). The cell search process must be performed periodically in order to update the cell to be connected to and to find a candidate cell for handover. The sync channel (SCH) and broadcast channel (BCH) are necessary for cell search. The 3GPP agreed to employ the Hierarchical SCH structure because the cell search time performance is of outstanding priority especially for handover cell search, conducted under very low signal to interference and noise ratio (SINR) conditions [2], [4].

There are many algorithms in the literature to do synchronization and cell search such as in [4]-[6]. In this paper, the effect of approximately all sync parameters and a combination between the accuracy and hardware simplicity will be taken into account.

We will follow the steps of [6]-[9] to distinguish between a fractional carrier frequency offset (FFO) being responsible for subcarrier misalignment and integer carrier frequency offset (IFO) being a multiple of the subcarrier spacing. The FFO can be estimated before the FFT demodulator (Pre-FFT) and the IFO can be estimated after FFT (Post-FFT). A non integer timing offset and /or sampling clock error cause(s) a drift in symbol timing and can further worsen the symbol synchronization problems. Thus, interpolators are implemented in a digital form using FIR filters. The main task of the interpolators is to calculate an intermediate values between known samples and then compensate the fractional timing offset (FTO) [10], [11]. The polynomial-based interpolation methods are the most widely used for performing the symbol timing adjustment in digital receivers due to the implementation efficiency of the hardware using the Farrow structure [10].

In this paper, we develop and investigate the performance of algorithms for the 3GPP LTE UE Digital Receiver (with free running RF oscillator) during call setup with the frequency division duplex (FDD) mode used in the downlink radio frame structure. The presented algorithms are discussed under channel impairments. These impairments comprise multipath Rayleigh fading channel, frequency offsets between eNode-Bs and UE (due to Doppler Effect and difference in both internal oscillators), time offsets, phase offsets, and additive white Gaussian noise (AWGN). The initial cell search procedure should be completed with high efficiency, low processing complexity at the UE, and within a very short time.

This paper is organized as follows: overview of some 3GPP LTE standards is given in section 2. MIMO-OFDM system model is presented in section 3. The proposed cell search procedure of the 3GPP LTE is presented in section 4. The proposed UE receiver architecture is discussed in section 5. Sync signals and proposed sync and cell identification algorithms are discussed in sections 6 and 7. Finally, results and conclusions are discussed in sections 8 and 9.

2 Overview of 3GPP LTE Standards
The following is a brief discussion of recent 3GPP LTE systems standards pertinent to the developed sync and cell search algorithms.

2.1 SCH Transmission Bandwidth

Scalable multiple transmission bandwidths are specified such as 1.25, 2.5, 5, 10, 15, and 20 MHz. The SCH is transmitted in the center of cell transmission bandwidth with the constant bandwidth of 1.25MHz regardless of the overall transmission bandwidth of the cell [3], [12].

2.2 Radio Frame Structure
In LTE downlink, the OFDM subcarrier spacing has been chosen as $\Delta f = 15\ kHz$. The sampling time T_s is $= 1/30720000$ sec, known as the basic time unit [2]. Figure (1) illustrates the downlink radio frame structure for 3GPP LTE transmission. There are two CP lengths defined for LTE, short (or normal) CP, and long (or extended) CP [3]. As shown in figure (1), each slot consists of 7 or 6 OFDM symbols in case of short or long CP, respectively. The useful symbol time $T_u = 1/\Delta f = 2048 \cdot T_s$ or $66.67\ \mu s$. The overall OFDM symbol time is the sum of the useful symbol time, T_u, and the CP length, T_{cp} or $T_{cp\text{-}e}$, as shown in figure (1). The basic LTE downlink physical resource in the time-frequency resource grid is called resource element which corresponds to one OFDM subcarrier during one OFDM symbol interval [2].
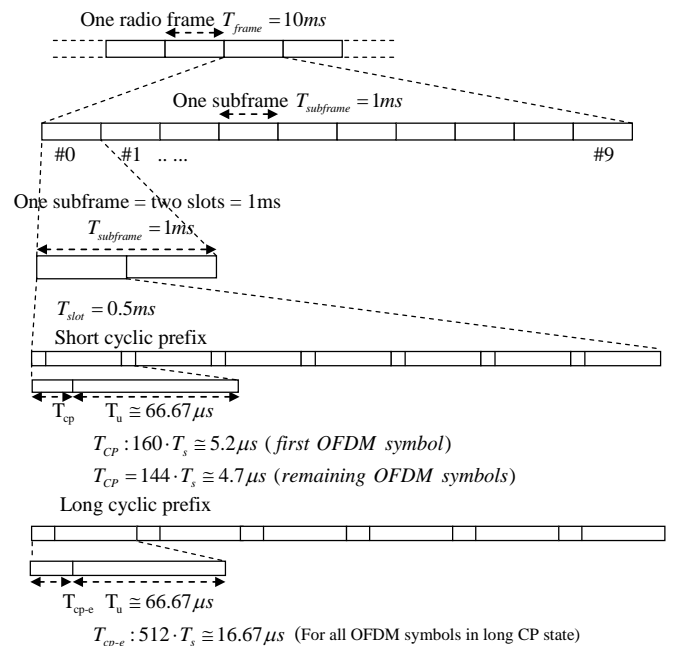

One radio frame $T_{frame} = 10ms$

One subframe $T_{subframe} = 1ms$

#0 #1 .. ...   #9

One subframe = two slots = 1ms

$T_{subframe} = 1ms$

$T_{slot} = 0.5ms$

Short cyclic prefix

T_{cp} $T_u \cong 66.67\mu s$

$T_{CP} : 160 \cdot T_s \cong 5.2\mu s$ (*first OFDM symbol*)

$T_{CP} : 144 \cdot T_s \cong 4.7\mu s$ (*remaining OFDM symbols*)

Long cyclic prefix

$T_{cp\text{-}e}$ $T_u \cong 66.67\mu s$

$T_{cp\text{-}e} : 512 \cdot T_s \cong 16.67\mu s$ (For all OFDM symbols in long CP state)

Fig. 1 Downlink frame structure of 3GPP LTE systems.

2.3 SCH Signals and Cell Identities
In LTE, adjacent cells are synchronized. That is, the frame starts in the neighboring cells coincide in time

to get the benefits of synchronized networks such as multicast broadcast single frequency network (MBSFN) and inter-cell interference management [3], [13].

3GPP LTE defines two sync signals: primary SCH (P-SCH), and secondary SCH (S-SCH). The grouping of cell identities, similar to that in W-CDMA, is applied to cell search in 3GPP LTE. There are 504 unique physical-layer cell identities, $N_{\text{ID}}^{\text{cell}}$. The cell identities are grouped into 168 unique cell-identity groups, each group containing three unique identities. A physical-layer cell-identity $N_{\text{ID}}^{\text{cell}} = 3N_{\text{ID}}^{(1)} + N_{\text{ID}}^{(2)}$ is thus uniquely defined by a number $N_{\text{ID}}^{(1)}$ in the range of 0 to 167 which can be detected from S-SCH, representing the physical-layer cell-identity group, and a number $N_{\text{ID}}^{(2)}$ in the range of 0 to 2 which can be detected from P-SCH, representing the physical-layer identity within the physical-layer cell-identity group [2]. Grouping of cell identities reduces the number of correlation detections. Therefore, after detecting $N_{\text{ID}}^{(2)}$ through P-SCH signal, only the cell-specific sequences of $N_{\text{ID}}^{(1)}$ belonging to the detected $N_{\text{ID}}^{(2)}$ are searched using S-SCH signals. A proposed reuse pattern of 3 for 3 P-SCH sequences is shown in figure (2).
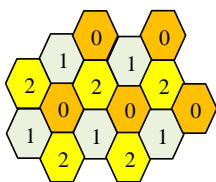

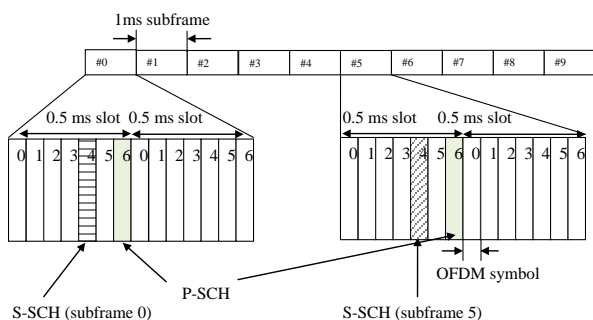Fig. 2 Pattern for reuse 3 P-SCH's.

Fig. 3 The positions of SCH OFDM symbols in FDD mode radio frame structure, assume short CP length.

For FDD mode (type 1) radio frame structure, the P-SCH shall be mapped to the last OFDM symbol in slots 0 and 10, and the S-SCH shall be mapped to the third last OFDM symbol in slots 0 and 10 [2]. Figure (3) shows the position of P-SCH and S-SCH OFDM symbols in FDD mode radio frame structure, which is considered in our

evaluation. Note that the P-SCH is transmitted twice in each frame. One reason is to simplify handover from other radio-access technologies such as GSM to LTE [14]. P-SCH symbols can only provide symbol timing but not frame timing due to the ambiguity of repetition the same P-SCH OFDM symbol. During detection of the S-SCH OFDM symbol, the terminal can obtain the frame timing due to the existence of two different S-SCH OFDM symbols in the frame.

3 MIMO-OFDM System Model

Figure (4) shows a typical MIMO-OFDM system model. The samples of the transmitted baseband MIMO-OFDM signal can be expressed as

$$x^p(n) = 1/\sqrt{N} \sum_{k=0}^{N_u-1} a_k^p e^{j2\pi kn/N} \; ; -N_{cp} \leq n \leq N-1 \quad (1)$$

where $p \in \{0,1\}$ denotes the antenna port of eNode-B, a_k^p is the subcarrier symbol mapped to antenna port p, N is the order of IFFT, $N_u \leq N$ is the number of useful subcarriers where the other subcarriers are padded by zeros in case of $N_u < N$, and N_{cp} is the number of CP symbols copied to the beginning of OFDM symbol to avoid inter-symbol interference (ISI) caused by multipath fading.

We consider a frequency selective multipath fading channel with path gains $\{h_l^{p,q} : l = 0,1,....,L_{path}-1\}$, including possible paths with a zero gain, where $h_l^{p,q}$ denotes the channel coefficient of path l between antenna port p in the eNode-B and antenna q in the UE based on Rayleigh distribution and the corresponding path delays $\{\tau_l\}$.
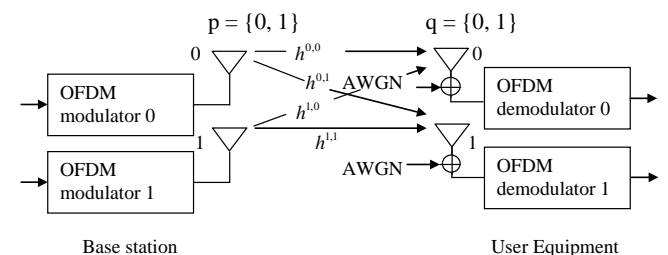

Fig. 4 MIMO-OFDM system, 2 antennas at the base station and the UE.

At the receiver, there exist carrier frequency offsets, sampling clock offset, and symbol timing offset, which have to be estimated and compensated. By assuming a perfect sampling clock, the received samples on UE antenna $q \in \{0,1\}$ become

$$r^q(n) = e^{j\theta} e^{j2\pi\gamma n/N} \sum_{p=0}^{1} \sum_{l=0}^{L_{path}-1} h_l^{p,q} x^p(n-\tau_l) + w^q(n)$$

(2)

where θ is an arbitrary carrier phase factor, γ is the carrier frequency offset normalized by a subcarrier spacing Δf, and $w^q(n)$ is a sample of a zero-mean complex Gaussian noise process with variance σ^2. It should be noted that the above equation considers integer timing offsets.

4 Cell Search Procedure

The objective of frequency sync is to establish subcarrier orthogonality as fast and accurate as possible (acquisition) and then maintain orthogonality as much as possible at all times during online reception (tracking). The following procedure presents the proposed cell search process.

(1) Stage 1 (Pre-FFT)

- Since phase information has not been obtained, non-coherent cross correlation detection is performed in the TD with 3 hypotheses of the P-SCH sequences to detect the OFDM symbol timing (FFT window timing) and $N_{ID}^{(2)}$.
- FFO is simultaneously detected.
- FFO using frequency de-rotator is corrected.

After stage 1, the UE would have identified $N_{ID}^{(2)}$.

However, $N_{ID}^{(1)}$ remains unknown to the terminal. The proposed algorithms use P-SCH in the TD to do non-coherent cross correlation which is also used in the FD to obtain channel gains for S-SCH.

(2) Stage 2 (Post-FFT)

- IFO is estimated in the FD.
- Coherent cross correlation detection in the FD with 168 hypotheses of the S-SCH sequences using a bank of correlators to detect $N_{ID}^{(1)}$.
- Detection of radio frame timing, based on the S-SCH which is transmitted twice every radio frame, within subframe 0 and 5, as shown in figure (3).
- FTO estimation using S-SCH and then fine timing synchronization.

After stage 2 the UE would have identified the physical-layer cell identity N_{ID}^{cell}, based on $N_{ID}^{(2)}$ from P-SCH and $N_{ID}^{(1)}$ from S-SCH. From the cell-identity N_{ID}^{cell}, the UE also obtains knowledge about which pseudo-random sequence is used for generating the reference signals in the cell [2].

Once the cell-search procedure is complete, the UE receives the broadcast system information to obtain the remaining parameters such as the transmission bandwidth used in the cell, the number of transmitting antennas and the type of CP based on BCH and reference signals. More details of the proposed synchronization and cell identification algorithms are given in section 7.

5 UE Receiver Architecture

Figure (5) shows a block diagram of the proposed UE digital receiver architecture involved in sync and cell search algorithms with two branch antenna diversity reception. It consists of the following units: Interpolator, sync signals generator, a set of hierarchical matched filters (HMFs) to do non-coherent cross correlation in the TD with the 3 P-SCH signals, a Pre-FFT detector to detect symbol timing and index of the received P-SCH, a carrier frequency estimator which consists of two units: FFO (useful in the TD), and IFO (useful in the FD), a carrier frequency correction unit with a frequency de-rotator, a removing CP and FFT window adjustment, FFT demodulator, a simple channel estimator for S-SCH referenced to P-SCH, a coherent cross correlators bank to do coherent cross correlation with the 168 S-SCH signals, a maximal ratio combining (MRC) over two received antennas [15], and a Post-FFT detector to detect index of S-SCH and frame timing. All units and their tasks are discussed in section 7.
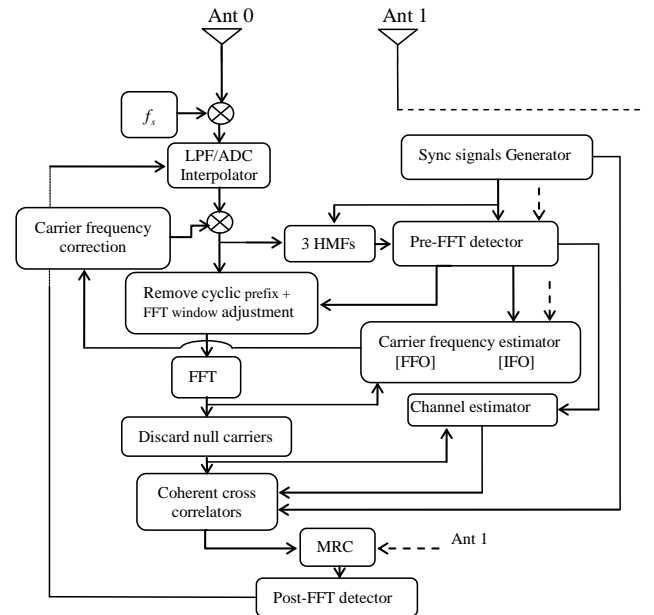

Fig. 5 The proposed UE receiver architecture.

6   Synchronization Signals

In wireless communication systems, the sync sequences are used to obtain initial estimation of sync parameters, and cell ID detection. They are designed to have the following desirable properties: large peak to side-lobe ratio (PSR) to simplify the detection process, low peak to average power ratio (PAPR) to limit the maximum transmit power of the cell [16], and the sync sequence should have constant amplitude zero autocorrelation (CAZAC) property which ensures efficient power amplifier utilization [8].

6.1 Primary Synchronization Signals

The P-SCH sequences, $d(n)$, are generated from a FD Zadoff-Chu sequence [17] which is a special case of generalized chirp like (GCL) sequence [18].

Based on the algorithm of P-SCH sequences generation in the 3GPP LTE evolved standard [2], each P-SCH sequence has one parameter: $N_{\mathrm{ID}}^{(2)} = 0$ or 1 or 2. For each sequence the magnitude is unity and the PAPR is 0 dB. For example, the autocorrelation of typical P-SCH sequence, $N_{\mathrm{ID}}^{(2)} = 1$, in the FD and the TD are shown in figure (6 - a, b), respectively. From figure (6), the PSR in the FD and TD are 5.293 and 10.632, respectively.
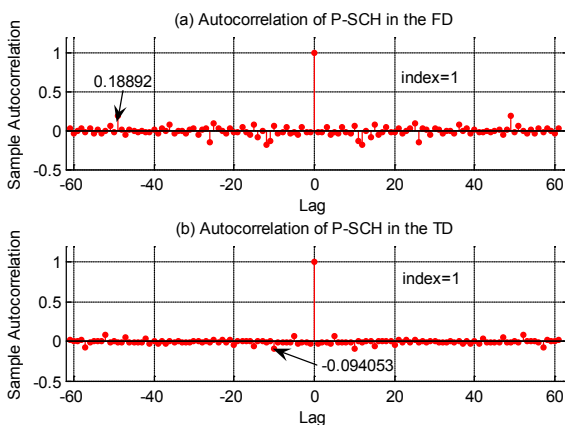

Fig. 6 The autocorrelation of typical P-SCH, $N_{\mathrm{ID}}^{(2)} = 1$ in (a) the FD (b) the TD.

6.2 Secondary Synchronization Signals

The design of the S-SCH sequences needs to support a sufficient number of hypotheses to carry 504 cell IDs jointly with the P-SCH sequences. The S-SCH sequence is an interleaved concatenation of two binary sequences of length-31. The combination of two length-31 sequences defining the secondary sync signal differs between subframe 0 and subframe 5. The concatenated sequence is

scrambled with a scrambling sequence given by the P-SCH. Based on the algorithm of S-SCH sequences generation in the 3GPP LTE evolved standard [2], each S-SCH sequence has three parameters: $N_{\mathrm{ID}}^{(1)} = 0$ or 1 or…167; $N_{\mathrm{ID}}^{(2)} = 0$ or 1 or 2; and its position in subframe 0 or 5. For each S-SCH sequence the magnitude is unity and the PAPR is 0 dB. For example, the autocorrelation of typical S-SCH sequence ($N_{\mathrm{ID}}^{(1)} = 19$, $N_{\mathrm{ID}}^{(2)} = 0$, and subframe 0) in the FD is shown in figure (7) where its PSR is 5.458.

In general, the considered SCH signals in the FD satisfy CAZAC property (approximately ZAC), i.e. PAPR = 0 dB. The 3 P-SCH sequences have PSR ranges from 6.44 to 12.858 in the TD and from 3.677 to 5.293 in the FD, and the 1008 (of subframe 0 and subframe 5) S-SCH sequences have PSR ranges from 4.170 to 12.392 in the TD and from 1.943 to 7.163 in the FD. The mean previous results of SCH sequences are summarized in table (1). It should be noted that the PAPR and PSR of the considered SCH signals substantially exceed the corresponding parameters of the GCL sequence which is more useful than other sequences such as Gold, and Golay sequences [16].
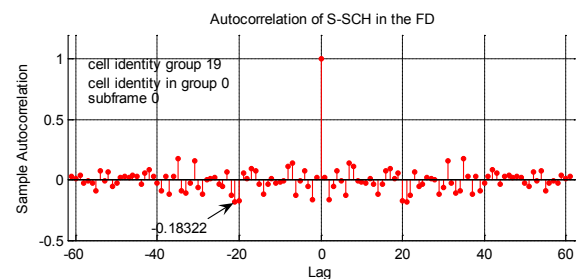

Fig. 7 The autocorrelation of typical S-SCH sequence ($N_{\mathrm{ID}}^{(1)} = 19$, $N_{\mathrm{ID}}^{(2)} = 0$, and subframe 0) in the FD.

Table 1 PAPR and PSR properties for SCH sequences.

Sequence	FD or TD	length	PAPR (dB)	PSR
P-SCH (3 sequences)	FD	62	0	4.617
	TD*	128	4.393	5.227
S-SCH (1008 sequences)	FD	62	0	3.967
	TD*	128	6.532	6.748
GCL (62)	FD	62	0	2.473

*eq. (1) is used ($N_u = 62$, $0 \le n \le N-1$) with minimum IFFT points of LTE ($N = 128$).

Based on the 3GPP LTE evolved standard [2], each sync sequence has a length of $L_{SCH} = 62$, and there are 5 subcarriers reserved and not used for transmission (set to zero) on each side of the sync sequence to generate the sync OFDM symbol [2], as shown in figure (8).
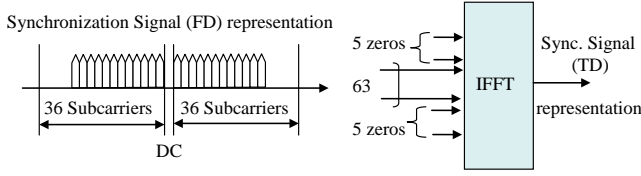

Fig. 8 Mapping the sync signal in the FD.

7 Proposed Synchronization and Cell Identification Algorithms

Both states of non-perfect sampling and perfect sampling will be discussed. For non-perfect sampling, a Farrow structure of order 3 and 4 will be used under oversampling by 4. Their coefficients can be found in [10]. The proposed algorithms in section 4 execute a complete synchronization and cell search procedure in two stages as follows

7.1 Stage1 (Pre-FFT)

The initial cell search algorithm performance will focus on a specific carrier frequency although international roaming and carrier frequency search is usually performed among more than 600 carrier frequencies [12].

Step a: Coarse Timing Synchronization and Physical-layer Cell-identity in Group Detection
The received samples are fed to HMFs which have three correlators per antenna, as shown in figure (5). A non-coherent cross correlation is performed between the received samples on both antennas with the known three types of P-SCHs in the TD over a length-N FFT window.

Square-law detection (SLD) is selected to measure the responses of the HMFs. Thus, the cross correlation between the received samples and P-SCH replicas, $c_{P-SCH,i}(u)$ where $i \in \{0,1,2\}$ corresponds to $N_{ID}^{(2)}$, in the TD at the UE receiver antenna q is represented as

$$D_1^{i,q}(n) = \left| 1/L_{SCH} \sum_{u=0}^{N-1} r^q(u+n) \cdot c_{P-SCH,i}^*(u) \right|^2 \quad (3)$$

where we divided by L_{SCH} for normalization. The cross correlation value in eq. (3) can be computed

every $N \times N_{oversamp}$ samples when oversampling is performed by $N_{oversamp}$.

After taking the maximum value from the three output correlators and its corresponding $P - SCH_{i=0or1or2}$, the computed correlation values of the two received antennas can be averaged over one radio frame in order to reduce the effect of noise and interference as much as possible. Also, the average correlation values of the two received antennas are further combined every correlation window. The base station with the highest peak correlation is selected as a candidate for further investigation. Thus, the symbol timing of the P-SCH OFDM symbol of the target cell from surrounding cells is detected as

$$\hat{n} = \max_n \{D_1^i(n)\} \quad (4)$$

where $\hat{n}$ is the estimated symbol timing parameter of the P-SCH OFDM symbol of the target cell over the repetition of 5ms, and the decision $D_1^i(n)$ is the average decision for the two antennas. In addition to maximizing $D_1^i(n)$, it should exceed a certain experimentally selected threshold to reduce the probability of error.

Step b: Fractional Frequency Offset Estimation (Pre-FFT Carrier Frequency Acquisition)
A normalized FFO estimate can be obtained based on the phase of the non-coherent cross correlation function results from the Coarse Timing Synchronization (step a above), using the coarse timing acquisition sample instant $\hat{n}$. The maximum likelihood (ML) frequency estimate based on the phase of autocorrelation of the received samples that are at a distance of N from each other over a length N_{cp} window becomes [7], [9], and [19]

$$\hat{\gamma}_{ML}^q = 1/2\pi \arg\left\{ \sum_{u=0}^{N_{cp}-1} r^*(u+\hat{n}) \cdot r(u+\hat{n}+N) \right\} \quad (5)$$

However, the ML frequency estimate based on the phase of cross correlation over N samples is

$$\hat{\gamma}_{ML}^q = 1/\pi \arg\left\{ \sum_{u=0}^{N-1} r^q(u+\hat{n}) \cdot c_{P-SCH,i}^*(u) \right\} \quad (6)$$

If oversampling is done by $N_{oversamp}$, eq. (6) becomes

$$\hat{\gamma}_{ML}^q = \frac{1}{\pi N_{oversamp}} \arg\left\{ \sum_{u=0}^{N \times N_{oversamp}-1} r^q(u+\hat{n}) \cdot c'^*_{P-SCH,i}(u) \right\}$$

$$(7)$$

where $c'^*_{P-SCH,i}(u)$ is a rectangular pulse shaped version of $c^*_{P-SCH,i}(u)$ with $N_{oversamp}$ samples per symbol. Averaging is done between two antennas to get $\hat{\gamma}_{ML}$. The frequency offset can then be corrected using frequency de-rotator from the received OFDM

symbol excluding CP by multiplying it with $e^{-j2\pi\bar{\gamma}_{ML}n/N}$; $0 \le n \le N-1$.

7.2 Stage 2 (Post-FFT)

Once coarse timing and FFO estimates are obtained, the received signal is corrected by the estimated values. Then, OFDM reception requires guard interval removal and FFT window adjustment, and converted into the FD as follows (see eq. (2)):

$$r^{q'}(n) = \{e^{j\theta}e^{\frac{j2\pi\gamma n}{N}}\sum_{p=0}^{1}\sum_{l=0}^{L_{path}-1}h_l^{p,q}x^p(n-\tau_l)+w^q(n)\} \times e^{-j2\pi\bar{\gamma}_{ML}n/N}$$

(8)

The FFT output of an effective OFDM symbol (excluding CP) is given by

$$Y^q(m) = \frac{1}{\sqrt{N}}\sum_{n=0}^{N-1}r^{q'}(n)e^{-j2\pi nm/N} \quad ; 0 \le m < L_{SCH}+10$$

$$Y^q(m) = \frac{1}{\sqrt{N}}\sum_{n=0}^{N-1}\{e^{-j2\pi\bar{\gamma}_{ML}n/N}e^{j\theta}e^{j2\pi\gamma n/N}\sum_{p=0}^{1}\sum_{l=0}^{L_{path}-1}$$

$$h_l^{p,q}x^p(n-\tau_l)+w^q(n)\times e^{-j2\pi\bar{\gamma}_{ML}n/N}\}\times e^{-j2\pi nm/N}$$

(9)

Let in eq. (9)

$$W^q(m) = 1/\sqrt{N}\sum_{n=0}^{N-1}w^q(n)\times e^{-j2\pi(\bar{\gamma}_{ML}+m)n/N}$$

(10)

Then, using eq. (10) & (1) in eq. (9) yields

$$Y^q(m) = \frac{1}{\sqrt{N}}\sum_{n=0}^{N-1}\begin{Bmatrix} e^{j2\pi(\gamma-\bar{\gamma}_{ML})n/N}e^{j\theta}\sum_{p=0}^{1}\sum_{l=0}^{L_{path}-1} \\ h_l^{p,q}\times 1/\sqrt{N}\sum_{k=0}^{N_u-1}a_k^p e^{j2\pi k(n-\tau_l)/N} \end{Bmatrix}$$

$$\times e^{-j2\pi nm/N}+W^q(m)$$

(11)

If the sync signals are considered, the two antennas in the eNode-B transmit the same SCH at the same time, thus, from eq. (11)

$$Y^q(m) = e^{j\theta}\sum_{k=0}^{N_u-1}H_k^q a_k \cdot \frac{1}{N}\sum_{n=0}^{N-1}e^{j2\pi(\gamma-\bar{\gamma}_{ML}+k-m)n/N}$$
$$+W^q(m)$$

(12)

where H_k^q is

$$H_k^q = \sum_{p=0}^{1}\sum_{l=0}^{L_{path}-1}h_l^{p,q}e^{-j2\pi k\tau_l/N}$$

(13)

Step a: Integral Frequency Offset Estimation

The residual frequency offset, that is an integer multiple (± 2 or more) of the subcarrier spacing, can be estimated by computing a cross correlation of $\{C_{P-SCH,i}^*(k)\}_{k=0}^{L_{SCH}-1}$ with its corresponding received sequence, where i is the index of received P-SCH. From eq. (12) the demodulated sync OFDM symbol is represented by eq. (14)

$$Y^q(m) = FFT_N\{r^q(n)e^{-j2\pi\bar{\gamma}_{ML}n/N}\} \; ; 0 \le m < L_{SCH}+10$$

(14)

The scanning cross correlation is performed using eq. (15).

$$\beta_j^q = \frac{1}{L_{SCH}}\sum_{k=0}^{L_{SCH}-1}Y^q(5+j+k)\cdot C_{P-SCH,i}^*(k)$$

(15)

where $j = -5,....,5$. The maximum absolute value of eq. (15) yields the IFO as follows

$$\hat{\Gamma}^q = \arg\max\{\|\beta_j^q\|\} \qquad ; j = -5,....,5$$

(16)

Averaging is also done between the two antennas of UE to get $\hat{\Gamma}$. It should be an integer number. The IFO can then be corrected using frequency de-rotator from the received OFDM symbol excluding CP by multiplying it with $e^{-j2\pi\hat{\Gamma}n/N}$; $0 \le n \le N-1$.

Step b: Initial Channel Estimation for S-SCH

The received P-SCH signal is used as a reference to compensate the channel variation for S-SCH signal. The 10 surrounding subcarriers are removed by discarding null carriers unit, see figure (5), to get $\{Y_{P-SCH,i}^q(m')\}_{m'=0}^{L_{SCH}-1}$. The channel gain is computed by averaging the neighboring three P-SCH signals with the subcarrier of S-SCH is in the center. The channel gains are computed as follows:

$$\{H^{'q}(m')\}_{m'=0}^{L_{SCH}-1} = \{Y_{P-SCH,i}^q(m')\}_{m'=0}^{L_{SCH}-1}/\{C_{P-SCH,i}(m')\}_{m'=0}^{L_{SCH}-1}$$

(17)

Let $\Upsilon(m') = \alpha_m.e^{-j\phi_{m'}}$ be the channel parameter and $\hat{\Upsilon}(m')$ be the estimate of $\Upsilon(m')$. Thus, the average channel gains are

$$\hat{\Upsilon}^q(m') = \{H^{'q}(m'-1)+H^{'q}(m')+H^{'q}(m'+1)\}/3$$ (18)

The output of each correlator is multiplied by the corresponding complex-valued (conjugate) channel gain $\{\hat{\Upsilon}^{q*}(m')\}$. The effect of this multiplication is to compensate for the phase shift in the channel and to weight the signal by a factor that is proportional to the signal strength. Thus, a strong signal carries a larger weight than a weak signal [20].

Step c: Physical-layer Cell-identity Group and Frame Timing Detection

Let $\{Y_{S-SCH}^q(m')\}_{m'=0}^{L_{SCH}-1}$, corrected from frequency offset based on the estimation from P-SCH, be the FD received sequence at the FFT timing $\hat{n}-2N-2N_{cp\ or\ cp-e}$, taking into consideration that this has been calculated from P-SCH timing ($\hat{n}$), see figures (1, 3). The complexity of the UE will be increased; as the cell ID identification process must be performed for each CP length, short and long.

Therefore, the CP length of the S-SCH at the third last OFDM symbol is estimated using blind detection.

Coherent detection is used in computing the decision variables using the estimated channel parameters [20]. The UE receiver correlates the L_{SCH} received samples with a replica of each S-SCH samples, $\{C_{S-SCH,i}(k)\}_{k=0}^{L_{SCH}-1}$ where $i \in \{0,..,167\}$ is the $N_{ID}^{(1)}$, multiplies each of the correlator outputs by the corresponding estimates $\{\widehat{\Upsilon}^{q*}(m')\}_{m'=0}^{L_{SCH}-1}$, and normalizes the resulting sum by L_{SCH} as follows

$$D_2^{i,q} = \text{Re}\left\{\frac{1}{L_{SCH}}\sum_{m'=0}^{L_{SCH}-1} Y_{S-SCH}^q(m') \cdot \widehat{\Upsilon}^{q*}(m') \cdot C_{S-SCH,i}^*(m')\right\} \quad (19)$$

Averaging over one radio frame or more by coherent summation to reduce the influence of the background noise and interference can be done. Furthermore, the correlation values of two receiver antennas are coherently combined by MRC. From the averaged decision D_2^i over the two antennas of UE, the S-SCH index, $N_{ID}^{(1)}$, of the target cell is identified as

$$\widehat{i} = \max_i(D_2^i) \quad (20)$$

Then the cell ID can directly be determined as follows:

$$N_{ID}^{\text{cell}} = 3N_{ID}^{(1)} + N_{ID}^{(2)} \quad (21)$$

Due to the existence of two different S-SCH sequences in the frame as shown in figure (3), the terminal can resolve the 5 ms timing ambiguity resulting from the first stage in the cell search procedure and determines the frame timing.

Step d: Fractional Timing Offset Estimation
Fine timing will be the last task in the acquisition process. Once the frequency offset is corrected, fine timing can be done by cross correlating the frequency corrected samples with the known SCH sequences. If the positive symbol timing offset ($\tau = \Delta n T_u / N$) exists in the received signal, the Post-FFT signal is then represented as follows [21]

$$Y(k) = e^{-j2\pi k \Delta n/N}\alpha(\Delta n)X(k) + W_\tau(k) \quad (22)$$

where the ISI and ICI are modelled as additional noise $W_\tau(k)$, and $\alpha(\Delta n)$ is the attenuation factor. $\alpha(\Delta n)$ is close to one for large N and can be neglected [9], [22].

The fine timing in FD is estimated from (19) as

$$\Delta \widehat{n}_{fine}^q = -N/(N_u\pi) \times \arg$$
$$\left\{\sum_{m'=0}^{L_{SCH}-1} Y_{S-SCH,i}^q(m') \cdot \widehat{\Upsilon}^{q*}(m') \cdot C_{S-SCH,i}^*(m')\right\} \quad (23)$$

Finally the net timing offset for the entire UE receiver over the two reception antennas $q = \{0,1\}$ is selected to be

$$\Delta \widehat{n}_{opt,fine} = 1/2\sum_{q=0}^1 \Delta \widehat{n}_{fine}^q \quad (24)$$

From (24), fine timing is estimated from S-SCH sequence of detected cell in the FD. Then, $\Delta \widehat{n}_{opt,fine}$ is used to control Farrow structure interpolator to compensate timing offset as [11]

$$\widehat{\mu} = \widehat{\tau}/T_s - \lfloor \widehat{\tau}/T_s \rfloor = 4\Delta\widehat{n}_{fine} - \lfloor 4\Delta\widehat{n}_{fine} \rfloor \quad (25)$$

where μ is a fraction which discretizes the sampling time T_s to certain discrete levels. It is a directly method to control the interpolator rather than a numerically controlled oscillator (NCO).
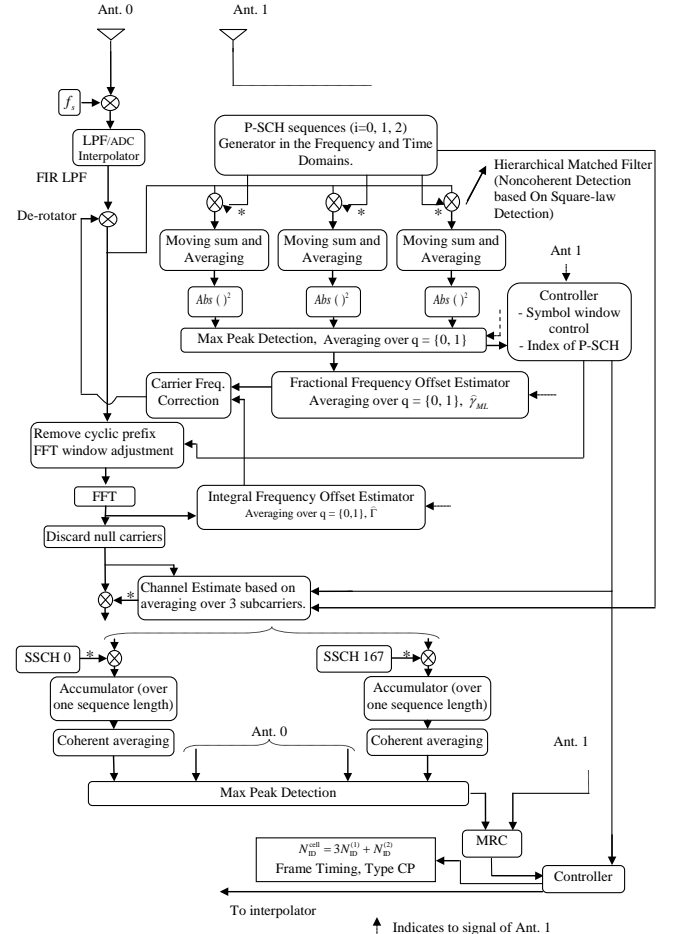

Fig. 9 A detailed proposed UE receiver.

Figure (9) shows a detailed functional block diagram of the proposed UE receiver involved in sync and cell search using the considered SCH structures. It should be noted that the proposed structure is free of any feedback loops to the analog

part of the UE receiver. This allows the design and verification of the digital and analog components independently.

8 Simulations and Discussions

Simulations were carried out to evaluate the proposed sync and cell search algorithms in 3GPP LTE systems. The simulation parameters are summarized in table (2). One and two transmit antennas of eNode-B are considered. If there are two antennas in eNode-B, the same SCH sequence is transmitted from both antennas at the same time, which is advantageous when performing synchronization. If continuous matched filtering is not performed, then oversampling can be used. Oversampling is also performed to measure its effect on the probability of correct cell identification in single cell and multi cell scenarios. SCH sequence is carried over 62 subcarriers and the length of null subcarriers is 5 in each side of SCH subcarriers, see figure (8). Therefore, the total number of useful subcarriers is 72 subcarriers occupying the central 1.25 MHz. It should be noted that the corresponding bandwidth for 72 subcarriers is 1.08 MHz. Thus, the unused subcarriers are placed at the edges of the useful spectrum. This lowers constrains on the analog filters at the eNode-B and UE. To modulate data in the physical downlink shared data channel, we used 16 QAM modulation based on [2].

The channel model adopted in [12], Extended Vehicular A model (EVA), is used with the vehicular speed 37.8 Km/hr and a maximum Doppler frequency $f_D = 70Hz$. The 3rd state of multi antenna channel models (SIMO=1×2, and MIMO=2×2) is used (low correlation between correlation matrices). In a frequency selective multipath fading channel model, each discrete path is considered as an independent Rayleigh fading channel with normalized multipath according to the Jake's spectrum [23]. A uniformly distributed frequency offset within $\pm 6\ kHz$ is used which corresponds to 3 ppm (3 part per million) at the 2 GHz carrier frequency. In multi cell scenario, the value of the frequency offset per cell is selected randomly, with uniform distribution, within $\pm 6\ kHz$. The position of UE in the multi cell scenario is selected randomly between cells and the corresponding far effect from the eNode-B's is taken into account. The timing in multiple cells is divided into two types: Inter-site synchronous, such that the frame starts in neighboring cells coincides in time, and Inter-site asynchronous such that the

frame starts in neighboring cells don't coincide in time. The two types are considered in simulation.

Table 2 Simulation Parameters

Carrier frequency f_c	2 GHz
Frame structure	FDD mode (Type1)
SCH Bandwidth	1.25 MHz
Sampling frequency	1.92 MHz
IFFT/FFT size	128/128
Subcarrier spacing Δf	15 kHz
Cellular Layout	Single cell site / Multi cell sites (Hexagonal grid)
ISD (inter-site distance) of Multi cell model	1732 m (1 km radius)
Doppler frequency f_d	70 Hz (speed 37.8 Km/hr)
Frequency offset f_{offset}	Uniformly distributed within ±6 kHz (3 ppm)
Number of antennas in eNode-B/ UE	1 or 2 / 2
Cyclic prefix	Short (normal)
Maximum time allowed for detection	2 frames (20 ms)
Order of oversampling	$N_{oversamp} = 2$ or 4 or 8
Type of channel	Rayleigh fading channel (EVA [12])
Thermal noise density	-174 dBm
Type of filter in eNode-B/UE	Rectangular Pulse Shaping / Low pass symmetric FIR

Digital low pass FIR filter is used in the UE to filter the received signal. The appropriate thresholds for two types of figures were selected experimentally; namely the probability of correct cell identification, P_c, in single cell and multi cell scenarios, and the probability of error detection IFO.

The $P_c's$ in single cell scenario are plotted in figure (10). The effect of one or two antennas in the eNode-B, and oversampling by $N_{oversamp}$ in the UE are shown. It should be noted that, when $N_{oversamp}$ increases, the P_c increases. For example at 0 dB, the P_c increases from 0.83 to 0.93, when $N_{oversamp}$ increases from 2 to 8. There is a huge improvement shown in figure (10) in the P_c when the number of antennas in the eNode-B increases from 1 (SIMO=1×2) to 2 (MIMO=2×2) especially at low SNR's. For example, at -6 dB P_c increases from 0.718 to 0.923 when $N_{oversamp}$ equals 4.
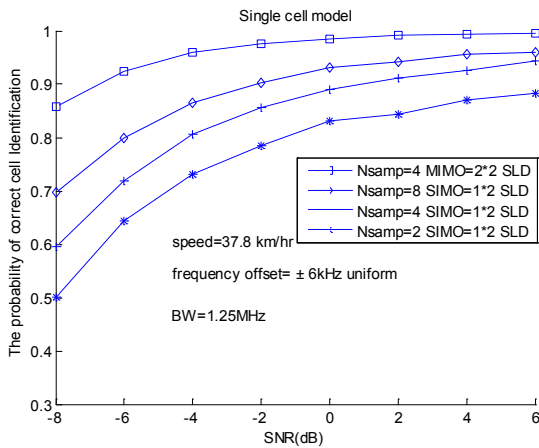
Fig. 10 The probability of correct cell identification in single cell model.
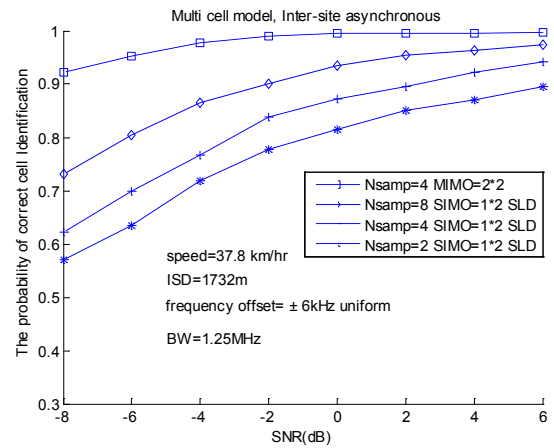
Fig. 12 The probability of correct cell identification in multi cell model (inter site asynchronous).
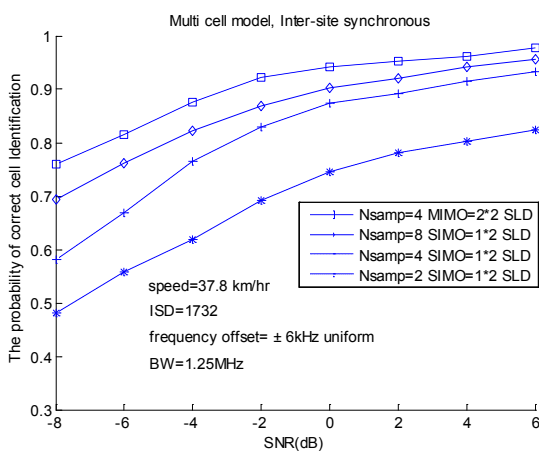
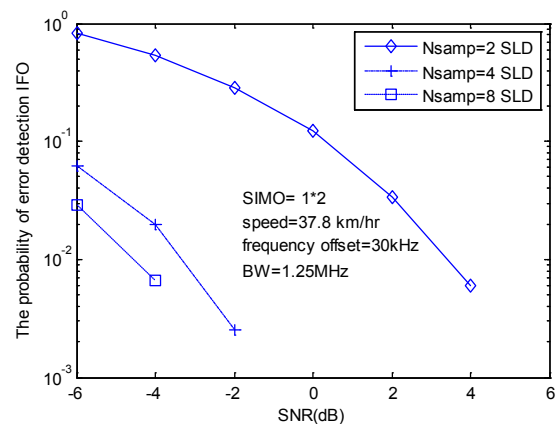Fig. 11 The probability of correct cell identification in multi cell model (inter site synchronous).

The same effect of oversampling and MIMO (2×2) in the P_c of single cell scenarios occurred in multi cell scenarios, with inter site synchronous or inter site asynchronous, as shown in figures (11, 12), respectively. The P_c's of inter site asynchronous networks are better than inter site synchronous networks due to coinciding frames in the inter site synchronous networks. The probability of error detection IFO ($30kHz$) is shown in figure (13), with single cell scenario. From figure (13), if the SNR is 0 dB and above, the probability of error detection IFO would be very small.

Finally, if there is a FTO (non-perfect sampling clock), an interpolator can be used to compensate it. For single cell scenario, the correct probability of cell identification is plotted in figure (14). Figure (14) has some different parameters comparing to the previous figures. Those are the range of frequency offset ±7.5 kHz ($±1/2 \Delta f$) rather than ±6 kHz and fractional timing offset between zero and worst point, both with uniform distribution. Figure (14)

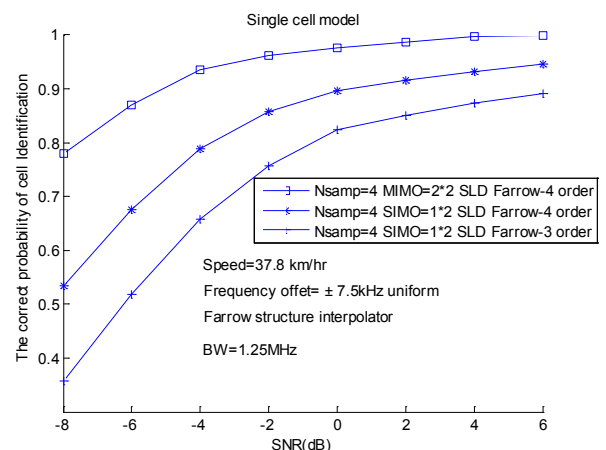Fig. 13 The probability of error detection IFO (30KHz).

Fig. 14 The correct probabilities of cell identification in single cell model, non perfect sampling clock (fractional timing offset).

shows some degradation at low SNR's comparing to the previous plots due to fractional timing offset when the cubic order is used, and it shows fine high probability as the previous plots at high SNR's. It shows also that the 4th order can do compensation

better than 3rd order Farrow structure interpolator in UE especially at low SNR's. For example at 0 dB, SIMO (1×2) and $N_{oversamp}$ equals 4, the P_c increases from 0.824 to 0.897, when the order of Farrow structure increases from 3 to 4. Figure 15 shows the correct probabilities of cell identification in multi cell model scenarios with non perfect sampling clock (fractional timing offset). It shows some degradation compared with the previous results due to the fractional timing offset.
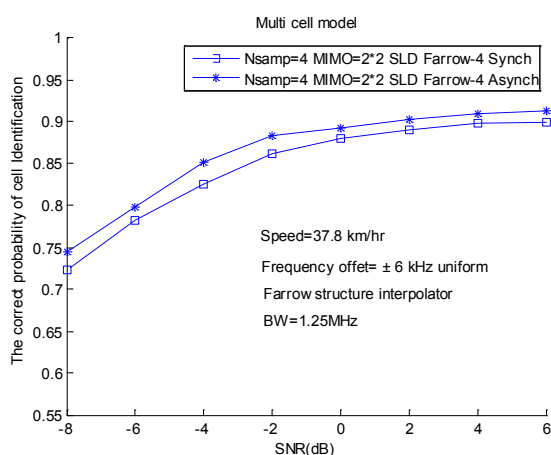

Fig. 15 The correct probabilities of cell identification in multi cell model, non perfect sampling clock (fractional timing offset).

9 Conclusions

This paper proposed user equipment (UE) receiver algorithms involved in cell search and synchronization (sync) with two branch antenna diversity reception for 3GPP LTE systems. Properties of primary and secondary sync signals such as peak to side-lobe ratio (PSR), peak to average power ratio (PAPR), and constant amplitude zero autocorrelation (CAZAC) are considered and seen to be better than those obtained using other sequences such as Gold, Golay, and generalized chirp like (GCL) sequences.

A robust symbol timing and carrier frequency sync methods in Rayleigh multipath fading environments have been presented. The acquisition of carrier frequency offsets both fractional frequency offset (FFO), and integral frequency offset (IFO) is presented. A Farrow structure interpolator is used to compensate the fractional timing offset (FTO) due to a non integer timing offset and /or sampling clock offset. The efficiency of the UE increases when the order of Farrow structure increases from 3 to 4 under oversampling by 4. The proposed cell search process can obtain

fast (20ms) and robust synchronization in multipath fading channels with large frequency offsets. The probability of correct cell identification in single cell and multi cell scenarios both inter site synchronous and inter site asynchronous networks can be improved using MIMO (2×2) technique, and/or over sampling at the UE.

References:

[1] 3GPP TR 25.913 V9.0.0, Requirements for Evolved UTRA (EUTRA) and Evolved UTRAN (E-UTRAN), Sep. 2009.

[2] 3GPP TS 36.211 V9.1.0, Physical Channels and Modulation, Mars 2010.

[3] 3GPP TR 25.814 V7.1.0, Physical layer aspects for evolved Universal Terrestrial Radio Access (UTRA), Sep. 2006.

[4] S. Nagata, Y. Kishiyama, M. Tanno, K. Higuchi, and M. Sawahashi, Cell Search Time Comparison Using Hierarchical and Non-Hierarchical Synchronization Channels in OFDM Based Evolved UTRA Downlink, *Vehicular Technology Conference IEEE 65th*, Vol., No., VTC 2007, pp. 1239-1244.

[5] M. Tanno, S. Nagata, Y. Kishiyama, K. Higuchi, and M. Sawahashi, Physical Channel Structures and Cell Search Method for Scalable Bandwidth for OFDM Radio Access in Evolved UTRA Downlink, *IEICE TRANS. COMMUN*, Vol. E90–B, No. 12, 2007, pp. 3622-3632.

[6] SU Huan, ZHANG Jian-hua, Cell search algorithms for the 3G long-term evolution, *THE JOURNAL OF CHINA UNIVERSITIES OF POSTS AND TELECOMMUNICATIONS (CHUPT),* Vol. 14, No. 2, 2007, pp. 33-37.

[7] Gordon L. Stüber, John Barry, Steve W. McLaughlin, Ye (Geoffrey) Li, Mary Ann Ingram, Thomas G, Broadband MIMO-OFDM Wireless Communications, *Proceedings of the IEEE*, Vol. 92, No. 2, 2004, pp. 271 – 294

[8] Hlaing Minn, Vijay K. Bhargava, and Khaled Ben Letaief, A Robust Timing and Frequency Synchronization for OFDM Systems, *IEEE TRANSACTIONS ON WIRELESS COMMUNICATIONS,* Vol. 2, No. 4, 2003, pp. 822-40.

[9] Michael Speth, Stefan Fechtel, Gunnar Fock, and Heinrich Meyr, Optimum Receiver Design for OFDM-Based Broadband Transmission—Part II: A Case Study, *IEEE TRANSACTIONS ON COMMUNICATIONS*, Vol. 49, No. 4, 2001, pp. 571-78.

[10] Heinrich Meyr, Marc Moeneclaey, Stefan A. Fechtel, *Digital Communication Receivers: Synchronization, Channel Estimation, and Signal Processing*, John Wiley & Sons, 1998.

[11] R. Hamila, J. Vesma, H. Vuolle, and M. Renfors , Joint Estimation of Carrier Phase and Symbol Timing Using Polynomial-Based Maximum Likelihood Technique, *IEEE International Conference on Universal Personal Communication*s, Vol. 1, No. , 1998, pp. 369–373.

[12] 3GPP TS 36.101 V8.3.0, User Equipment (UE) radio transmission and reception, Sep. 2008.

[13] 3GPP TS25.211 V8.6.0, Physical channels and mapping of transport channels onto physical channels (FDD), Dec. 2009.

[14] Erik Dahlman, Stefan Parkvall, Johan Sköld and Per Beming, *3G EVOLUTION: HSPA AND LTE FOR MOBILE BROADBAND*, ELSVIER, 2007.

[15] Brenan, D.G., Linear Diversity Combinig Techniques, *Proc. IRE.,* Vol. 47, No. 6, 1959, pp. 1075-102.

[16] Yingming Tsai, Guodong Zhang, Donald Grieco, Fatih Ozluturk, Cell Search in 3GPP Long Term Evolution Systems, *IEEE VEHICULAR TECHNOLOGY MAGAZINE*, Vol. 2, No. 2, 2007, pp. 23-29.

[17] D.C. Chu, Polyphase codes with good periodic correlation properties, *IEEE Trans. Inform. Theory*, Vol. 18, No. , 1972, pp. 531–32.

[18] B.M. Popovic, GCL polyphase sequences with minimum alphabets, *IEE Electronics Letter*, Vol. , No. 4, 1994, pp. 106–07.

[19] T. Schmidl and D. Cox, Robust frequency and timing synchronization for OFDM, *IEEE Trans. Commun.*, Vol. 45, No. 12, 1997, pp. 822-39.

[20] John G. Proakis, *Digital Communications*, MC Graw Hill, 2001.

[21] Hanli Zou, Bruce McNair, and Babak Daneshrad, An Integrated OFDM Receiver for High-Speed Mobile Data Communications, *IEEE Global Telecommunications Conference*, Vol. 5, No. , 2001, pp. 3090–3094.

[22] Michael Speth, Stefan A. Fechtel, Gunnar Fock, and Heinrich Meyr, Optimum receiver design for wireless broad-band systems using OFDM Part-I, *IEEE trans. Com.,* VOL. 47, NO. 11, 1999.

[23] Jakes, *Microwave Mobile Communications*, Wiley, 1974.

Abdo N. Gaber received the B.S. degree in Electronics and Communications from Sana'a University, Sana'a, Yemen in 2005, and M.S. degree supported by DAAD in Communications from the University of Jordon, Amman, Jordan in 2009. He worked in Sabafon Comm. Company as a BSS engineer in 2005-2006 and MTN Comm. Company in 2009-2010 as a transmission supervisor. Currently, he is working in his PHD in Positioning Systems in Otto –Von- Guericke University Magdeburg, Germany. His research interests include wireless communication systems.

Loay D. Khalaf Received the M.S. and Ph.D. degrees in Electrical Engineering from Georgia Institute of Technology. Loay held several senior positions at Nortel, Scientific Atlanta, NEC, and Telematix, where he worked on Fiber Loop Carriers, cable TV, CDMA cellular systems, and WLAN. Currently, he is on the faculty of the University of Jordan. His research interests include design and development of communication systems.

Ahmad M. Mustafa received the B.S. degree in Industrial Electronics from Munofia University, Egypt in 1972. After working for the Royal Scientific Society (RSS) of Jordon, Amman for 6 years he obtained the M.S. and Ph.D. degrees in communications from Ohio State Univ. (OSU), Columbus, Ohio in 1982 and 1985, respectively. In 1985 he joined the faculty of the Electrical Engineering Department of the University of Jordon, Amman, as an assistant professor. His research interests include wireless communication systems, remote control and tracking using existing mobile/wireless networks. Dr. Ahmad is a senior member of the IEEE Society since 2004.